



Functionalized Electrolytic Manganese Dioxide Nanostructure Prepared at Fixed pH for Electrochemical Supercapacitor

Hadi Adelhkani^z

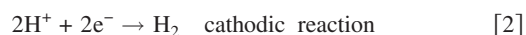
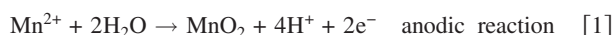
Material Research School, Nuclear Science and Technology Research Institute, Tehran (098)21, Iran

MnO₂ samples are synthesized by an electrodeposition technique at a fixed pH and are tested as active electrode material for an electrochemical supercapacitor. The physicochemical properties of electrolytic manganese dioxide, including average Mn oxidation state, amount of incorporated water, porosity, crystal structure, morphology, and electrochemical performance, are characterized. The characterization is carried out by thermal gravimetry, composition analysis, the Barrett–Joyner–Halenda model, X-ray diffraction, scanning electron microscopy, and cyclic voltammetry methods. The correlation between these properties and the deposition conditions (pH) is studied. The results show that the pH strongly influences the properties and, consequently, the activity of MnO₂ in an electrochemical supercapacitor.

© 2009 The Electrochemical Society. [DOI: 10.1149/1.3184344] All rights reserved.

Manuscript submitted May 6, 2009; revised manuscript received June 25, 2009. Published July 31, 2009.

Manganese dioxide (MnO₂) is one of the most attractive materials due to its catalytic, ion-exchange, magnetic, and electrochemical properties.^{1–5} It is used especially as an electrode material in batteries and supercapacitors because of its energetic compatibility in a reversible electrochemical system.^{4,7} Electrolytic manganese dioxide (EMD) can be produced by an electrolysis of an aqueous solution of MnSO₄. The electrodeposition of EMD is overlapped by the oxidation (Reaction 1) and reduction (Reaction 2) of species on the anode and the cathode, respectively^{5,6}



According to the anodic/cathodic reactions, the generation of excess H⁺ ions is an inherent part of EMD electrodeposition. It leads to a large decrease in the pH value and to a change in the electrodeposition conditions and the properties of EMD deposits.^{6,7} In a previous paper, we adjusted the pH at 2 and 5 and then characterized the samples. The results confirmed that the pH of the solution has remarkable effects on the nanostructure, crystal structure, porosity, and the electrochemical performance of the EMD as a cathode in rechargeable alkaline manganese dioxide batteries. The aim of this paper is to extend previous research and to characterize the manganese dioxide samples that were prepared at fixed pH (2, 3, 4, 5, and 6). The chemical composition, micro- and nanostructures, porosity (surface area, pore size, and pore-size distribution), and electrochemical performance of MnO₂ as an active material in supercapacitors are studied by attention to pH value.

Experimental

The EMD samples were produced from a solution containing MnSO₄ (0.74 mol L⁻¹) at a temperature of 80°C and an anodic current density of 0.8 A dm⁻². A titanium plate was used as the anode (area: 1 dm²) between two Pb plates that were used as the cathodes (area: 2 dm²). The pH of the solution was monitored in situ by a pH meter. Five samples were electrodeposited at fixed pH 2, 3, 4, 5, and 6 by adding NH₄OH (10%). They are named M2–M6, as shown in Table I.

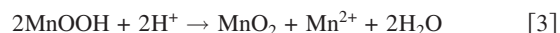
The chemical composition of the samples was determined using the potentiometric titration approach of Vetter and Jaeger⁸ based on the cation vacancy model proposed by Ruetschi.⁵ The surface water content was determined by heating a sample in air in an oven at 110°C for 2 h. After cooling to ambient temperature in a desiccator, the weight reduction was measured. For the determination of structural water, the sample was then heat-treated at 400°C and reweighed. The Ruetschi cation vacancy fraction is also an indicator of the level of structural defects within γ-MnO₂. The cation va-

cancy, Mn(IV) and Mn(III), species can be calculated from the structural water (% H₂O_{st}) and total manganese content (% Mn_t) of the sample. Detailed descriptions of calculations can be found in the previous works.⁵

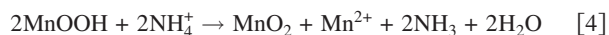
Powder X-ray diffraction (XRD) analysis was carried out by using a Philips X-ray diffractometer (Cu Kα radiation, 30 kV). Scanning electron microscopy (SEM), Philips model XL30, was used to study the morphology of the samples. The pore-size distribution was determined using a desorption isotherm by the Barrett–Joyner–Halenda (BJH) method (BELSORP-mini II, BEL Japan). Cyclic voltammetry (CV) experiments were carried out using the three-electrode system consisting of a saturated calomel electrode (SCE), a Ti plate, and a MnO₂ composite material as reference, counter, and working electrodes, respectively. The working electrode was prepared by mixing 70% MnO₂ powder, 20% graphite (conducting grade), 5% acetylene black, and 5 wt % poly(tetrafluoroethylene) dried powder. The mixture was mounted onto a Ti grid current collector to form an electrode disk (area: 1 cm²) that consisted of 3 mg of MnO₂. Electrochemical tests were performed with the aid of a potentiostat/galvanostat (Kimiastate model 210) instrument in a Na₂SO₄ solution between –100 and 900 mV vs SCE.

Results and Discussion

Material characteristics.—XRD.—The X-ray patterns of the samples (Fig. 1) confirm that MnO₂ was obtained at all pH regardless of the presence of H⁺ or NH₄⁺. This result is in line with the possible complete disproportion reaction in low or high pH to produce MnO₂. The electrodeposition of manganese dioxide is believed to consist of multisteps that MnOOH produced and is disproportionated in the steps. MnOOH is unstable in an acidic environment and is disproportionate



Instead of Reaction 3, in the presence of NH₄⁺ ions another disproportion reaction (Eq. 4) can occur⁹



Such Mn(III) seems to be disproportionate to produce MnO₂ according to Reactions 3 and 4. In other words, regardless of the presence of H⁺ or NH₄⁺, the disproportion reactions occur (Reactions 3 and 4).

In proportion to the acidity of the solution, the intergrowths of α-MnO₂ or β-MnO₂ possibly occur in γ-MnO₂. Previous studies have confirmed that the mixtures of β/γ-MnO₂ and α/γ-MnO₂ were obtained at high and low pH, respectively. The intensive diffraction peaks at 2θ ≈ 22, 37, 43, 56, and 65–68° could be assigned to the characteristic peaks for γ-MnO₂. The peaks that occurred at 2θ ≈ 28, 49, and 60° should be ascribed to the characteristic peaks for α-MnO₂. The presence of β-MnO₂ is verified by a shift in the peak at 2θ ≈ 22° to a higher angle and a sharper peak at 2θ ≈ 56°. ^{5,6}

^z E-mail: hadelkhani@aeoi.org.ir; adelkhani@hotmail.com

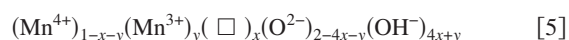
Table I. The electrodeposition pH conditions of prepared samples, pore volume, and mean pore diameter of the samples.

EMD sample	M2	M3	M4	M5	M6
pH	2	3	4	5	6
BJH V_p pore volume ($\text{cm}^3 \text{g}^{-1}$)	0.017	0.024	0.012	0.010	0.151
Total pore volume (BET) ($\text{cm}^3 \text{g}^{-1}$)	0.0318	0.043	0.0296	0.0224	0.152
Mean pore diameter (BET) (Å)	23.34	23.82	19.50	17.36	92.54

Seemingly, $\alpha\text{-MnO}_2$ is gradually eliminated and $\beta\text{-MnO}_2$ occurs by increasing pH from 2 to 6. M2 consists of $\alpha\text{-MnO}_2$. There is no $\alpha\text{-MnO}_2$ in other samples. It was confirmed that $\alpha\text{-MnO}_2$ was produced at lower pH.⁶

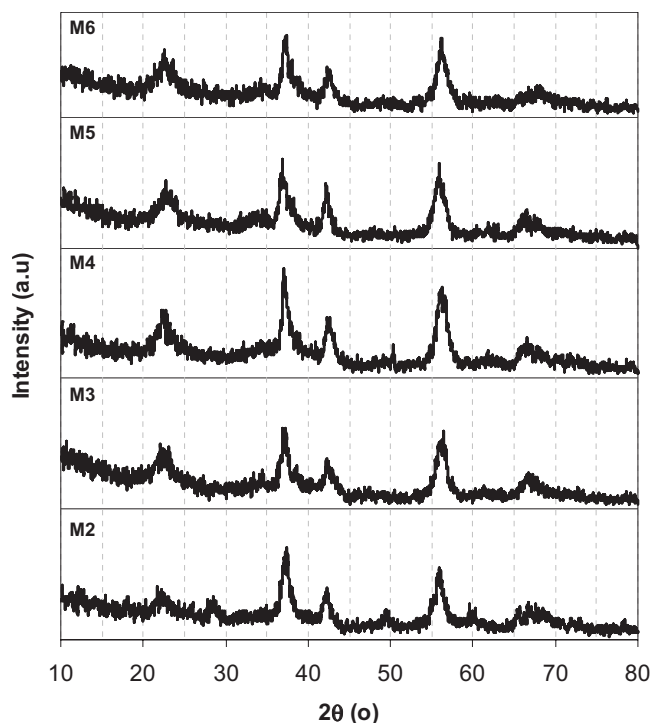
M5, in addition to the pure phases, consists of $\beta\text{-MnO}_2$. This is observed by a shift in the peak at $2\theta \approx 22^\circ$ to a higher angle and a sharper peak at $2\theta \approx 56^\circ$. Figure 1 shows that the XRD pattern of sample M4 is very similar to that of M5, the only significant difference being the sharper peak at $2\theta \approx 22^\circ$ indicating a lower amorphous and defective material.

Chemical composition.— It is confirmed that the average oxidation state of manganese is slightly less than (4+) so that one infers the presence of some Mn^{3+} or proton in the material. The cation vacancy model accounts for this structural variety. This structure can be written, following the Ruetschi formalism, as⁵



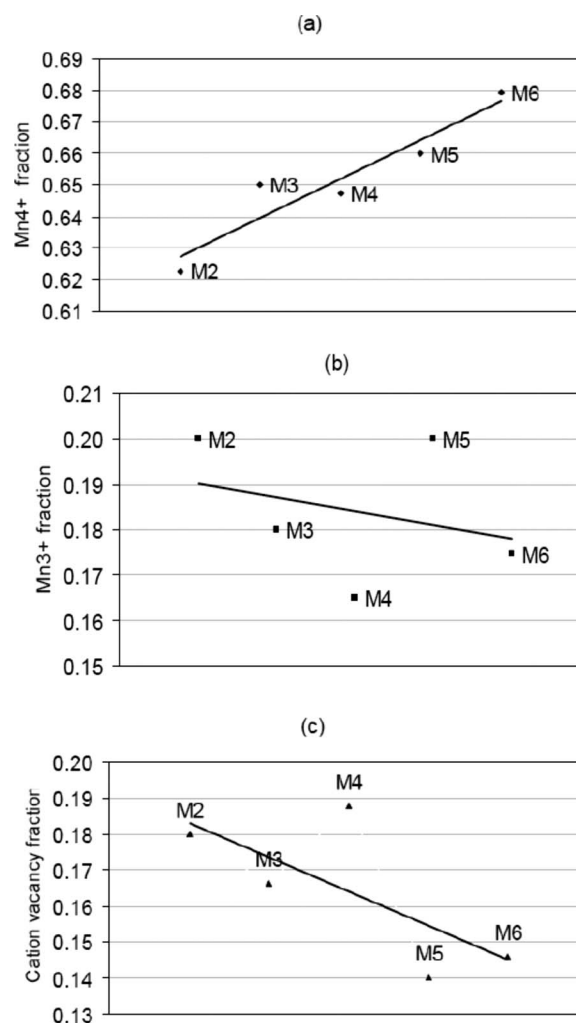
In this formula, protons (as water) are included to compensate the missing 4+ charges due to the Mn^{4+} vacancies and also the missing 1+ charge wherever Mn^{3+} replaces Mn^{4+} in the manganese lattice. (\square) is the cation vacancy. When $x = y = 0$ (no cation vacancies, no Mn^{3+}), the formula reduces to stoichiometric MnO_2 .

The fractions of cation vacancies Mn^{3+} and Mn^{4+} of samples are shown in Fig. 2. The fraction of Mn^{4+} has an increasing trend with increasing pH of the solution. Clearly, any cation vacancy within the structure is available through the removal of Mn^{4+} ions and the insertion of a proton. Hence, an opposite trend was observed for cation vacancy. The amount of Mn^{3+} species is also decreased with increasing pH.

**Figure 1.** XRD pattern of EMD samples prepared at different pH values (Table I).

In a relatively higher acidic solution (lower pH), the probability of dissolving Mn^{4+} is increased and the incorporation of Mn^{4+} ions into the lattice is decreased. Meanwhile, the fraction of cation vacancy increases with an increase in the acidity of the electrolyte solution.

The water content is proportional to the presence of proton in EMD, and it certainly plays a role in the electrochemical activity of EMDs (discussed in the next section). The water contents of samples are presented in Fig. 3. We show bilateral relations between the chemical composition (Fig. 2) and the water content (Fig. 3). The water content of M4 is higher than those of other samples, as is cation vacancy fraction. In addition, Mn^{3+} fraction of M4 is lower than those of other samples. Therefore, the H^+ ions in this sample are increased to obtain the charge equilibrium. The higher level of cation vacancies in M4 is related to the higher amount of physical water and to the easier transport of protons, replacing Mn^{4+} ions. In M2, however, the cation vacancy fraction is relatively high, but the

**Figure 2.** Effects of pH on chemical compositions of EMD samples prepared at different pH values (Table I): (a) Mn^{4+} fraction, (b) Mn^{3+} fraction, and (c) cation vacancy fraction.

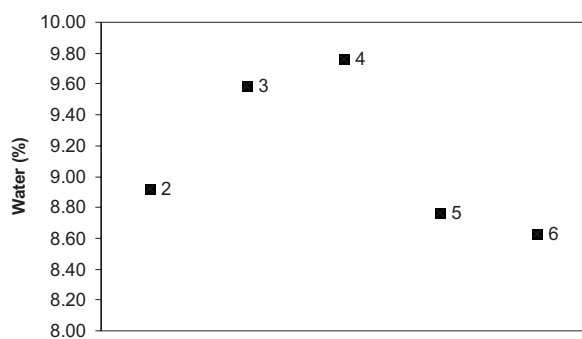


Figure 3. Effects of pH on the water content of EMD samples prepared at different pH values.

presence of the Mn^{3+} cation compensates for the missing charge. Consequently, this sample has a lower water content relative to M4. In M6, the water content is lower than other samples. M6's higher Mn^{4+} fraction seems to cause its low water fraction.

Morphological properties.—In this section, the effect of pH on morphology is studied. Figures 4a-e and 5a-e present the low and high magnifications of SEM photographs of the samples that were prepared from solutions with pH 2–6, respectively. In Fig. 4a-e, each sample exhibits a particular morphology. The samples electrodeposited at pH 2, 3, and 6 are thistlelike, mosslike, and reticulate, respectively. M4 and M5 have a textilelike appearance. Clearly, the SEM images in high magnification (Fig. 5a-e) show that the

shape and the particle size of MnO_2 samples, in a nanometer scale, are significantly changed by pH variation. This could be explained by considering the intermediates that were produced during the electro-oxidation of Mn^{2+} to MnO_2 . The formation of oxygen-containing intermediate Mn(III) species (e.g., MnOOH , $[\text{Mn}(\text{OH})_6]^{3+}$, and Mn_2O_3) is inevitable during the electro-oxidation of Mn^{2+} to MnO_2 . The physicochemical stability of these species plays an important role in the morphology of EMD by the inhibition grain growth mechanism on the anode/electrolyte interface.^{5,6,10,11} The Mn_2O_3 or MnOOH species are thermodynamically stable in higher pH, and they dissolve in a lower pH solution.

When the pH value was fixed at 2, the formed samples had a specific thistlelike morphology. Under a higher magnification (Fig. 5a), the structure is composed of a new nucleus or small nanograins of EMD that are formed on the surface of thistlelike structures. The morphology of this deposit clearly shows that at pH 2, by decreasing the stability and thickness of passive layers, the growth of crystal grains can be increased to produce multibranching thistlelike structures (see Fig. 5a).

At pH 3, an algae-like morphology was obtained. It shows an irregular morphology with large grains within fine ones (Fig. 5b). This sample also shows many nanocavities or nanoholes. The holes under the upper layer provide a high surface area due to high porosity. The M3 grains appear to bond together, and there is a high level of interconnected porosity. The average grain size (estimated from SEM micrographs) appears to be about 100 nm.

Figures 4c and d, 5c, and d show the morphology of EMD deposits at pH 4 and 5, respectively. The microstructures of two

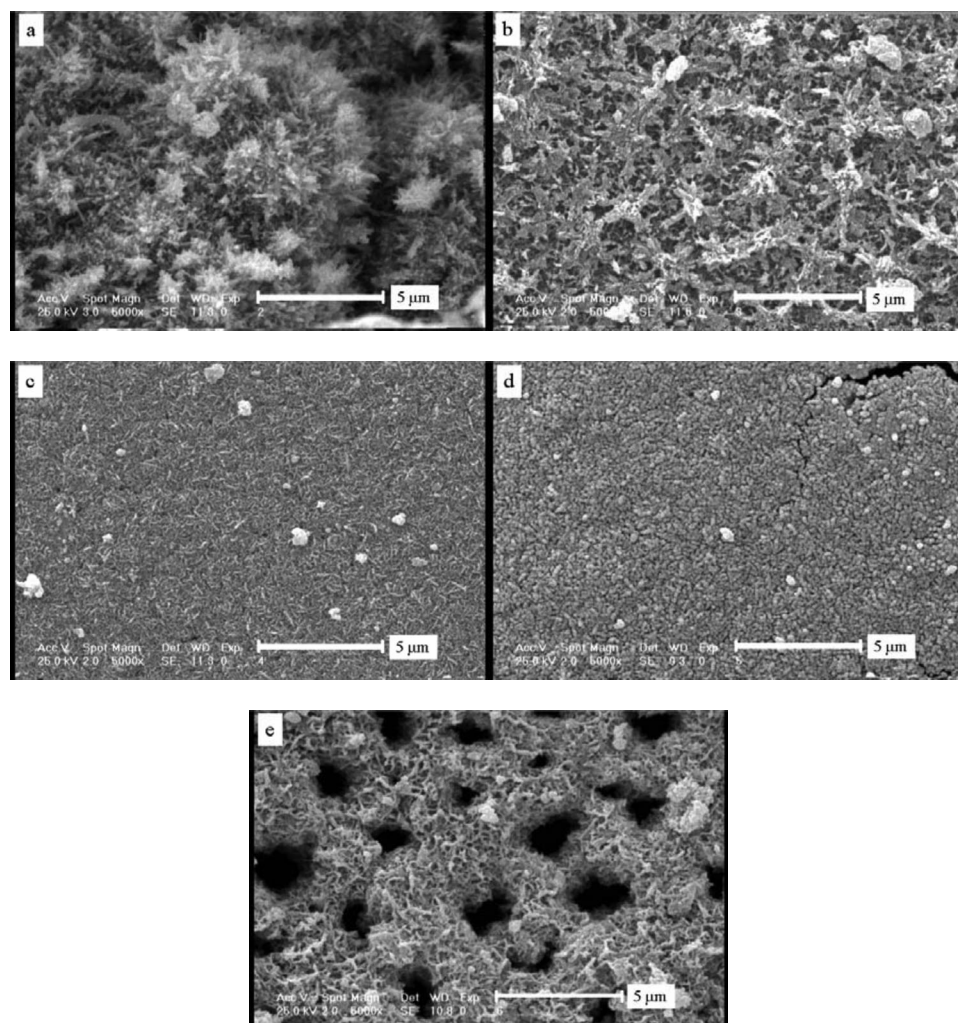


Figure 4. SEM images of EMD samples prepared at different pH values: (a) pH 2, (b) 3, (c) 4, (d) 5, and (e) 6.

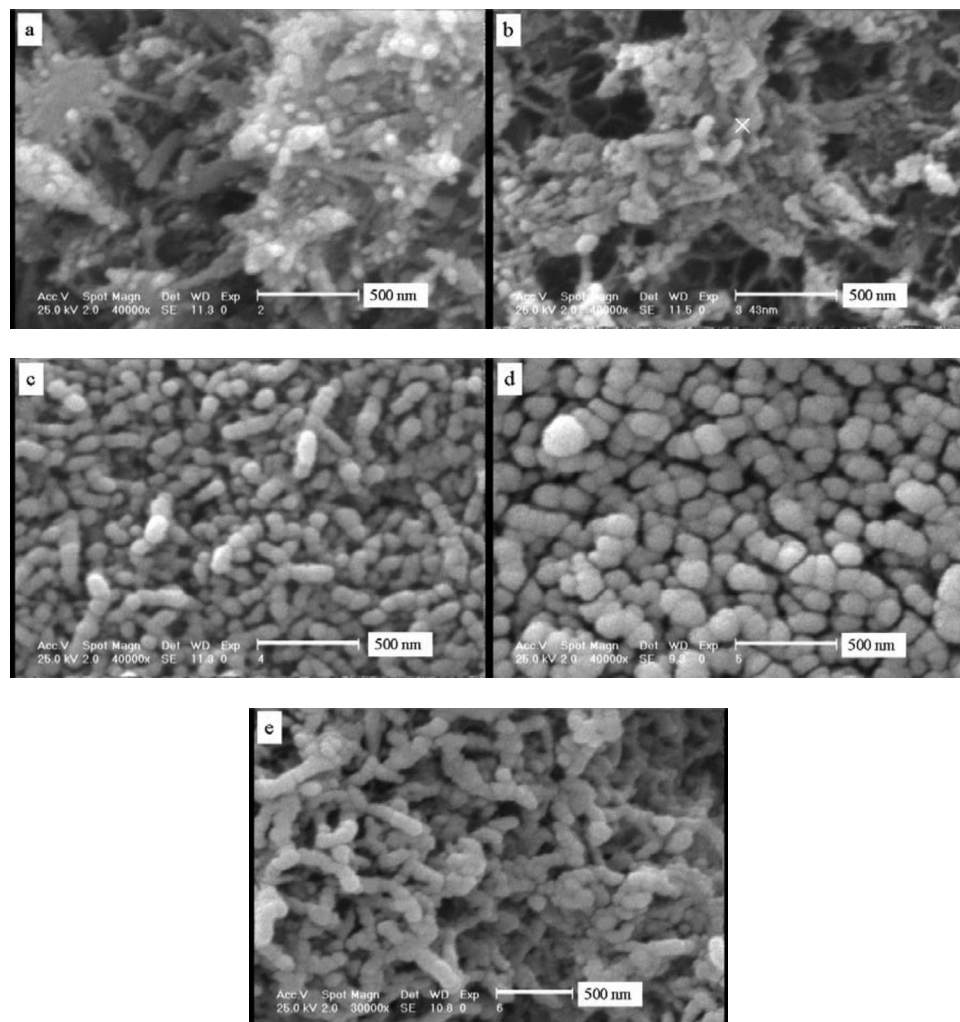


Figure 5. SEM images of EMD samples prepared at different pH values: (a) pH 2, (b) 3, (c) 4, (d) 5, and (e) 6.

samples that were prepared at pH 4 and 5 are very similar. They have uniform microstructures with textilelike agglomerates of fine particles under low magnification (Fig. 4c and d). Their difference can be distinguished at a higher magnification value SEM (Fig. 5c and d). Under a higher magnification, the structures of M4 and M5 are composed of nanocolumns and nanospheres of EMD, respectively. In M4, the diameter of columns is in the range of 7–8 nm and their length is on the order of 60–70 nm. In M5, the crystal growth is limited and nanoparticles are obtained. M5 demonstrates a uniform morphology consisting of nanospheres (\varnothing : 140 nm). The morphology of this deposit clearly shows a highly nanostructured and three-dimensional network. At a higher pH, the grain growth is prevented because of the higher stability of the Mn(III) species and the increasing thickness of the passive layers. This condition leads to several grains that have similar appearances, as seen in Fig. 5d. These two samples have a rigid structure, and so their porosities are low.

As shown in Fig. 4e, there are many holes on the sample that are prepared at pH 6 (M6). At pH 6, the grain growth is prevented because of the higher stability of the Mn(III) species and the increasing thickness of the passive layers. This condition leads to the production of holes on the surface of samples. As shown in Fig. 4e, M6 consisted of regularly distributed cellular pores of 1.5–2 μm in diameter. The pore walls are built from nanoparticles with an average diameter of about 100 nm (Fig. 5e). The voids between these particles form a continuous and nanohole wall structure. In this way, dual porosity (macro- and mesopores) is induced, which could fa-

cilitate fast cation (H^+ or Na^+) or electrolyte diffusion and mass transport. It is expected to produce the high electrochemical performance when used for capacitor applications.

Electrochemical properties.— CV is considered an appropriate tool to indicate the capacitive behavior of any material. Therefore, CV was carried out for all samples. All the CV (not shown) curves clearly show the rectangular and symmetric current–potential in anodic and cathodic directions that indicate a capacitive behavior. There are clearly no redox peaks in the range between -100 and 900 mV vs SCE.

The specific capacity of samples is calculated from the CV data, and the effect of the scan rate on it is presented in Fig. 6. A drastic decrease in the specific capacity as a function of the scan rate is seen for all samples. The dependence of capacity on scan rate can be explained with respect to the mechanism of charge/discharge in an electrochemical supercapacitor. A decrease in specific capacitance at a high scan rate is due to some polarization, indicating that all the electrode materials are not fully charged or discharged due to limited ionic diffusion in the electrode. At a low scan rate, the specific capacity of the samples is clearly high and corresponds to the sum of double-layer and faradaic contributions. One explanation is that such a low rate does not limit the diffusion of Na^+ ions and/or protons throughout the whole volume of the MnO_2 electrode, and consequently all pores and voids remain accessible at low sweep rates.

Another important point is the effect of pH on the specific ca-

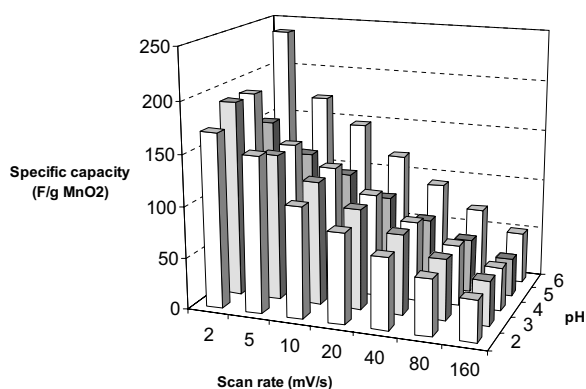


Figure 6. Specific capacitance of MnO₂ electrodes calculated from CV against the scan rate.

capacity. With respect to Fig. 6, M5 and M6 have lower and higher capacities, respectively. The study of physicochemical properties of EMD samples has shown that besides water content and their crystal structure, superior high power performance is linked to the morphology, especially on porosity (specific surface area, pore volume, and pore-size distribution) of MnO₂.^{12,13} The porosity is a critical property for high capacitance per volume and weight in supercapacitors. Therefore, the porosity of samples is calculated by the BJH method, and the results are presented in Fig. 7 and Table I.

The comparison of capacities for all samples indicates that the capacity of M6 is much more than that of other samples (Fig. 6). With respect to Fig. 7 and Table I, M6 shows a considerably larger pore volume and mean diameter than the other samples. The average pore diameter of the M6 material is 4 times larger than that of the other samples. Consequently, the pore volume of M6 was 0.152 cm³ g⁻¹, whereas it was in the range of 0.01–0.02 cm³ g⁻¹ for other samples. A larger pore volume could facilitate the mass transfer of cations, and it could lead to the augmentation of accessible electrochemical active sites during charge/discharge cycling.

With respect to Fig. 6, Table I, and Fig. 7, it is understood that M3, which has a lower porosity than M6, shows a capacity better than those of other samples, except M6. The morphology of M3 also consists of nanoholes (Fig. 4b and 5b). The improved performance of M3 could be attributed to the enhanced accessible active site of the material. Subsequently, even at high scan rates, a higher concentration of working ions is still able to access the active regions of MnO₂ active sites, so a decrease in the pseudocapacitance takes place to a much lesser extent.

Comparing M2 and M4, although the porosity of M2 is higher than M4, the latter shows a higher capacity. Another important factor is the water content of the electrode material. It is well recognized that the water content of manganese dioxide is one of the key factors in the electrochemical performance of MnO₂. The hydrous regions in the electrode provide the kinetically facile sites needed for the charge-transfer reaction and cation diffusion.¹⁴

Compared to M2, the higher specific capacitance of M4 is attributed to the higher amount of physically adsorbed water molecules and their contribution in the diffusion process (Fig. 4). M4 has a higher cation vacancy than M2, which may be another reason for the higher capacity of M4 compared to other samples.

Despite an enhanced morphology and porosity in M2 in comparison to other samples (M3, M6, and M4), the presence of α -MnO₂ may be the main reason for its lower capacity. It was reported that the presence of α -MnO₂ has a positive effect when the cycle life of the electrode is important.⁶

In M5, the condition is different. This sample has lower porosity and water content relative to other samples. Therefore, it is supposed that M5 shows the least capacity. The limitation observed in the M5 electrode highlights the importance of the ionic diffusion throughout

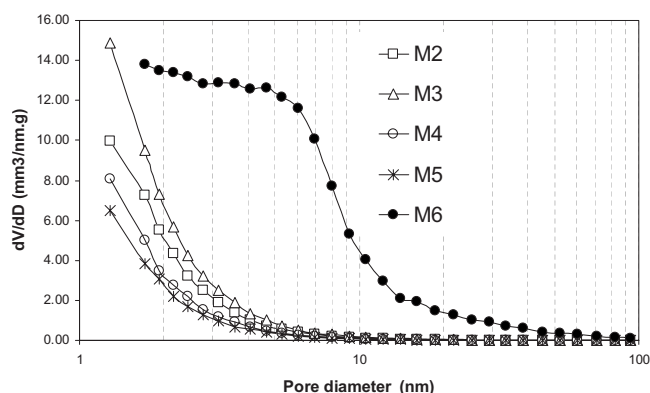


Figure 7. The BJH adsorption dV/dD vs pore volume.

the electrode. However, as depicted in Fig. 5d, at pH 5 the MnO₂ particles tend to agglomerate rather than form many particles. In M5, a slower ionic transport occurs within the active material, or protons cannot diffuse freely across the thickness of the MnO₂ particle.

Conclusion

In this paper, the crystalline structure, morphology, porosity, and electrochemical properties of manganese dioxide have been studied as a function of the electrolyte acidity (pH). The results show that one of the biggest advantages of electrodeposition at fixed pH is the ability to easily control the physicochemical properties and, consequently, the electrochemical performance of MnO₂. By SEM, the particle shape and size and, consequently, the dimensions and distribution of the resulting pores of the MnO₂ samples can be changed and controlled with a variation in the pH value of the electrolyte. The formation of oxygen-containing intermediate species (e.g., MnOOH, [Mn(OH)₂]³⁺, and Mn₂O₃) and their stability at different pH values lead to the production of excellent structures.

The different specific capacitances of manganese dioxide electrodeposited at different pH values are attributed mainly to their different water contents, porosities, and microstructures. The EMD, which was electrodeposited at pH 6 (M6), performed well in electrochemical capacitor applications. The large capacitance exhibited by this sample arises from its morphology and porosity. The comparison of capacities for all samples indicates that the accessible surface sites of M6 are much more than those of other samples. Manganese dioxide prepared at pH 6 was highly porous. Large regions of regular and homogeneous holes with diameters of about 1.5–2 μ m are formed under pH 6. The average primary particle size is about 100 nm. This results from the higher stability of the passive layer at pH 6.

References

- M. S. El-Deab and T. Ohsaka, *J. Electrochem. Soc.*, **153**, A1365 (2006).
- Q. H. Zhang, S. Sun, S. Li, H. Jiang, and J. G. Yu, *Chem. Eng. Sci.*, **62**, 4869 (2007).
- B. Tang, G. Wang, L. H. Zhuo, and J. Ge, *Nanotechnology*, **17**, 947 (2006).
- P. Ragupathy, H. N. Vasan, and N. Munichandraiah, *J. Electrochem. Soc.*, **155**, A34 (2008).
- H. Adelhani, M. Ghaemi, and S. M. Jafari, *J. Power Sources*, **163**, 1091 (2007).
- H. Adelhani and M. Ghaemi, *J. Alloys Compd.*, **481**, 446 (2009).
- O. M. S. Filipe and C. M. A. Brett, *Talanta*, **61**, 643 (2003).
- K. J. Vetter and N. Jaeger, *Electrochim. Acta*, **11**, 401 (1966).
- I. Tari and T. Hirai, *Electrochim. Acta*, **27**, 149 (1982).
- Z. Rogulski, H. Siwek, I. Paleska, and A. Czerwinski, *J. Electroanal. Chem.*, **543**, 175 (2003).
- S. Nijjer, J. Thonstad, and D. M. Haarberg, *Electrochim. Acta*, **46**, 395 (2000).
- S. C. Pang, M. A. Anderson, and T. W. Chapman, *J. Electrochem. Soc.*, **147**, 444 (2000).
- S. M. Davis, W. L. Bowden, and T. C. Richards, *J. Power Sources*, **139**, 342 (2005).
- M. Ghaemi, F. Ataherian, A. Zolfaghari, and S. M. Jafari, *Electrochim. Acta*, **53**, 4607 (2008).